within the optical waveguide. In Fig. 3 the achieved optical phase shift for a TE mode at a wavelength of 1·06 μm is compared with theory,[2] which implies electro-optic, electro-refraction and free carrier effects for the refractive index change. Note that, on account of the electric decoupling, a lateral confinement factor of 70% is ascertained to consider the confining of the effective modulated area to the waveguide region. With the achieved maximum phase shift of 370°/mm, coupling lengths down to 850 μm could be completely switched.

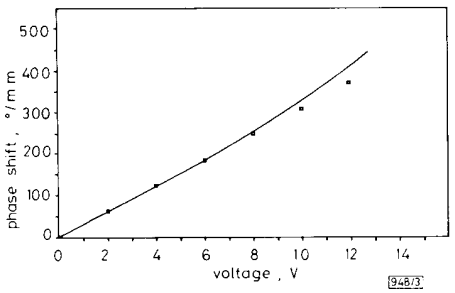

Fig. 3 *Optical phase shift characteristic for TE modes at λ = 1·06 μm*
Curve shows theory, squares show measured results

In conclusion, a properly designed delta doping layer reduces essentially the lateral current between adjacent DH waveguides and thus the power consumption. Beyond that, the at least quadratic potential drop along the parasitic field-effect transistor channel significantly reduces the effective area of the *pn* junction capacitance to the area of the optical waveguide. In general, such a design is well suited for microwave modulation and monolithic integration.

We thank Prof. Müller, H. W. Geiger, H. Rauch, R. Rodemeier, U. Penning and P. Unger for helpful discussions and device preparation. This work was supported by the Deutsche Forschungsgemeinschaft.

R. BAUER *25th September 1989*
Lehrstuhl für Technische Elektronik
Technische Universität München
Arcisstrasse 21, D-8000 München 2, Federal Republic of Germany

G. WEIMANN
Walter Schottky Institut
Technische Universität München
Arcisstrasse 21, D-8000 München 2, Federal Republic of Germany

W. SCHLAPP
Forschungsinstitut der Deutschen Bundespost
Postfach 5000, D-6100 Darmstadt, Federal Republic of Germany

References

1 FEIST, J., REINHART, F. K., and MARTIN, D.: 'Comparison of phase modulation of GaAs/AlGaAs double heterostructures', *Electron. Lett.*, 1987, **23,** pp. 1392–1393
2 MENDOZA-ALVAREZ, J. G., COLDREN, L. A., ALPING, A., YAN, R. H., HAUSKEN, T., LEE, K., and PEDROTTI, K.: 'Analysis of depletion edge translation lightwave modulators', *J. Lightwave Technol.*, 1988, **LT-6,** pp. 793–807
3 TAKEUCHI, H., NAGATA, K., KAWAGUCHI, H., and OE, K.: 'GaAs/AlGaAs directional coupler switch with submillimetre device length', *Electron. Lett.*, 1986, **22,** pp. 1241–1243
4 TAKEUCHI, H., KASAYA, K., and OE, K.: 'Low-switching voltage InGaAsP/InP waveguide interferometric modulator for integrated optics', *IEEE Photonics Technol. Lett.*, 1989, **PTL-1,** pp. 227–229
5 BULMAN, G. E., ROBBINS, V. M., and STILLMAN, G. E.: 'The determination of impact ionization coefficients in (100) gallium arsenide using avalanche noise and photocurrent multiplication measurements', *IEEE Trans.*, 1985, **ED-32,** pp. 2454–2466
6 SZE, S. M.: 'Physics of semiconductor devices' (Wiley, NY, Chichester, 1981)

GaInAs/GaInAsP MULTIPLE-QUANTUM-WELL INTEGRATED HETERODYNE RECEIVER

Indexing terms: Optoelectronics, Optical receivers, Semiconductor lasers, Optical communications

We describe the fabrication and performance of the first integrated heterodyne receiver capable of actual heterodyne data reception. Integrating a continuously tunable 1·5 μm MQW-DBR laser with a single-mode directional coupler/switch and zero-bias MQW waveguide photodetectors, we have achieved error-free reception of FSK-modulated pseudorandom digital code at 105 Mbit/s.

Photonic integrated circuits (PICs) are expected to become increasingly important in future lightwave systems where multiple, serially connected optical devices are required. One potentially important example is coherent transmission and networking, where integrated heterodyne receivers may be desirable. Previous work towards this goal includes narrow-line tunable sources with integrated parallel input ports and directional coupler switches,[1] directional couplers with integrated balanced detectors,[2] and very recently a tunable DFB laser with a coupler and detectors where a beat note was even observed.[3]

In this letter we describe the fabrication and performance characteristics of the first integrated heterodyne receiver PIC capable of actual heterodyne data reception. The device integrates a continuously tunable 4-section multiple-quantum-well (MQW) distributed-Bragg-reflector (DBR) laser with a parallel input port, feeding a directional coupler/switch followed by a pair of MQW waveguide detectors in a balanced receiver configuration. Rough sensitivity measurements with only one arm of the receiver indicate a 10^{-9} BER with 105 Mbit/s FSK reception at powers at least as low as ~ -32 dBm of waveguide-coupled power, or ~ -27 dBm of free-space beam power before the simple objective used for coupling.

The structure of the 3 mm-long heterodyne receiver PIC is shown in Fig. 1. The passive guides and the directional coupler employ low-loss semi-insulating InP clad, high-definition etch-stop-controlled buried rib waveguides, while the detectors and laser employ a semi-insulating-blocked buried heterostructure (SIPBH) design[4] for low capacitance and good current confinement. The continuously tunable local oscillator (LO) laser is a 4-section version of the previously described 3-section MQW-DBR laser,[5] with a 400 μm MQW gain section, a 100 μm phase section, a 300 μm high reflector Bragg near the PIC cleaved facet, and a 80 μm partial Bragg reflector internal to the PIC. We obtain in this PIC continuous access to a ~60 Å range at 1·53 μm, and thresholds range from ~20–35 mA. The 180 μm-long detectors employ for absorption the same MQW layers used for gain in the laser. Previous work indicates that good absorption efficiency

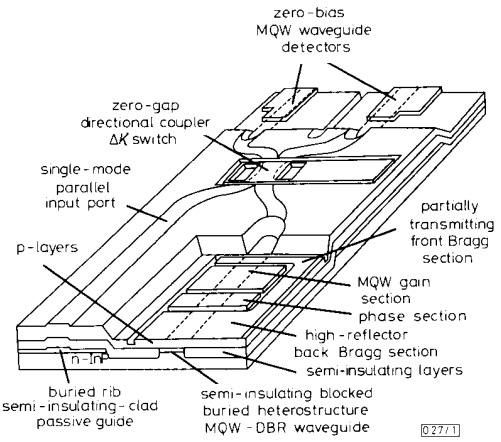

Fig. 1 *Configuration of integrated heterodyne receiver PIC*

is possible with such a detecting medium, and that out to at least ~5 GHz there are no significant speed problems from hole-trapping in the GaInAs/GaInAsP MQW system.[6] While the detectors were used here with no bias, a slight improvement of ~1 dB is observed with a reverse bias of ~0·5 V when mA-level photocurrents are generated by the LO laser. The coupler/switch is similar to that in a previously described MQW-DBR/switch PIC,[1] but here does not provide full switching. For the particular PIC used in the transmission result, a coupling ratio of 1·2 : 1 with no bias was used. In typical chips the combined photocurrent from the MQW detectors reaches ~1 mA into 50 Ω at laser drives of ~75–100 mA.

Fabrication of this PIC followed a variant of a previously described MOCVD-based processing sequence P-Pro2 using wet etching with etch-stop layers for precise depth control.[1,7] The original base wafer growth, up through the passive 1·3 μm GaInAsP core and the MQW active layer, also includes etch-stop layers for the MQW removal, buried rib definition and deep mesa formation for the buried heterostructure regions. The MQW active layer itself consists of four 80 Å GaInAs quantum wells with 100 Å 1·3 μm bandgap GaInAsP barriers. Following the longitudinal processing, including active layer removal and holographic grating formation, SiO_2 waveguide patterns are formed. Deep mesas are then etched for the laser and detector, while shallow rib guides are etched for the switch and passive guides. The SiO_2 is removed except in the laser and detector portions, and a semi-insulating InP blocking layer sequence is grown to provide lateral current confinement in the laser and detector regions and low-loss cladding and current rejection in the passive guides and switch. Current injection channels are etched in the coupler/switch region, and the SiO_2 is then removed over the lasers and detectors. A final *p*-type growth for the upper cladding and contact layers is then performed, including etch-stop layers for electrical isolation grooves. Following contact formation and isolation etches, the sample is cleaved into the 3 mm lengths of the PIC.

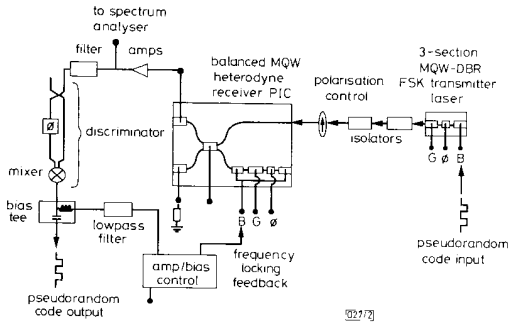

Fig. 2 *Experimental set-up for narrow-deviation FSK receiver operation*

The operation of the integrated heterodyne receiver PIC was evaluated using the experimental set-up shown in Fig. 2. The input signal was generated from a 3-section MQW-DBR laser transmitter which was FSK-modulated by applying pseudorandom code to the Bragg section. The signal passed through two isolators and polarisation control to match the LO on the receiver PIC, and was focused into the parallel input port using a long working distance ×40 objective AR-coated for the visible. While the heterodyne signal was observable on both arms, only one detector output passed through amplification into the discriminator circuit while the other detector was terminated into 50 Ω as shown in Fig. 2. The tunable LO was electrically tuned to match the transmitter and locked with a feedback circuit to an intermediate frequency (IF) specified by the adjustable phase of the discriminator; typical IF values were 500–700 MHz. Both the transmitter and the receiver PIC are temperature controlled at ~20°C. With the locking circuit disengaged, we observe very smooth, continuous tuning of the IF with no tendency either to injection-lock or to freeze due to any internal reflections in the receiver PIC. The beat signal shown in Fig. 3*a* is locked at a 700 MHz IF, and the 20 MHz/div, 5 dB/div trace shows a combined −3 dB beat width of 13·6 MHz, rising in this case >40 dB from the noise floor.

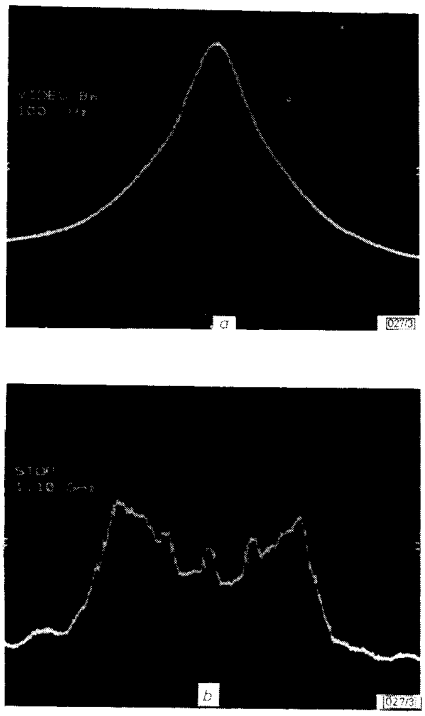

Fig. 3

a Electrical power beat spectrum from detector with no modulation applied to transmitter; 20 MHz/div horizontally and 5 dB/div vertically, with −3 dB width of 13·6 MHz

b Electrical power beat spectrum from detector with attenuated transmitter with pseudorandom 105 Mbit/s NRZ FSK modulation applied; 100 MHz/div horizontally and 5 dB/div vertically

With 105 Mbit/s NRZ modulation applied, FSK IF spectra are shown in Fig. 3*b* are obtained, here shown at 100 MHz/div, 5 dB/div with the IF locked at 600 MHz. In this Figure the input signal has been attenuated to ~−32 dBm of waveguide-coupled power, or about ~−27 dBm of free-space beam power prior to the simple coupling objective used here. The eye diagram at this signal level is shown in Fig. 4, and with a $2^{15} - 1$ pseudorandom code we obtain $< 10^{-9}$ BER. The bit rate at present is limited by the transmitter FM bandwidth. We expect significant improvements in sensitivity with AR coatings, improved coupling into the input guide, and most importantly the use of low-noise electronics with both

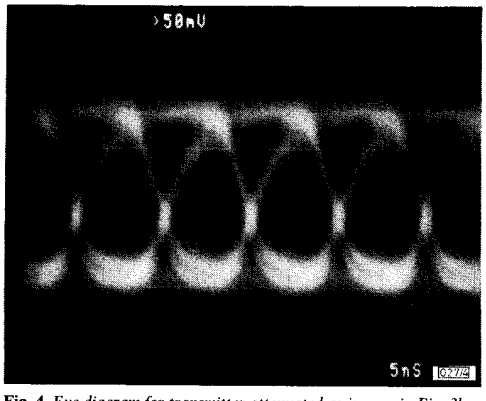

Fig. 4 *Eye diagram for transmitter attenuated as in case in Fig. 3b, with* $< 10^{-9}$ *BER*

detectors appropriately subtracted to remove LO intensity noise and utilise all the available power.

In closing, we feel that the prospects for further refinement and practical implementation of PICs of this type are quite good. We would also like to thank B. Glance and O. Scaramucci for assistance in setting up the FSK discriminator circuitry.

T. L. KOCH
U. KOREN
R. P. GNALL
F. S. CHOA
F. HERNANDEZ-GIL†
C. A. BURRUS
M. G. YOUNG
M. ORON
B. I. MILLER

AT&T Bell Laboratories
Holmdel, NJ 07733, USA

† Visiting from Telefonica Investigacion y Desarrollo, Lerida 43, 28020 Madrid, Spain

9th October 1989

References

1 HERNANDEZ-GIL, F., KOCH, T. L., KOREN, U., GNALL, R. P., and BURRUS, C. A.: 'Tunable MQW-DBR laser with monolithically integrated GaInAsP/InP directional coupler switch', *Electron. Lett.*, 1989, **25**, pp. 1271–1272

2 CHANDRASEKHAR, S., CAMPBELL, J. C., STORZ, F. G., DENTAI, A. G., JOYNER, C. H., and QUA, G. J.: 'Balanced dual photodiodes integrated with a 3dB directional coupler for coherent lightwave receivers', *ibid.*, 1988, **24**, pp. 1457–1458

3 TAKEUCHI, H., KASAYA, K., KONDO, Y., YASAKA, H., OE, K., and IMAMURA, Y.: 'Monolithic integrated optical circuit for coherent detection'. Tech. dig., 7th int. conf. on integrated optics and optical fiber commun., IOOC '89, Kobe, Japan, 1989, **5**, Postdeadline paper 20PDB-6, pp. 48–49

4 KOREN, U., MILLER, B. I., EISENSTEIN, G., TUCKER, R. S., RAYBON, G., and CAPIK, R. J.: 'Semi-insulating blocked planar BH GaInAsP/InP laser with high power and high modulation bandwidth', *Electron. Lett.*, 1988, **24**, pp. 138–140

5 KOCH, T. L., KOREN, U., GNALL, R. P., BURRUS, C. A., and MILLER, B. I.: 'Continuously tunable 1·5 μm multiple-quantum-well GaInAs/GaInAsP distributed-Bragg-reflector lasers', *ibid.*, 1988, **24**, pp. 1431–1433

6 CHOA, F. S., KOCH, T. L., KOREN, U., and MILLER, B. I.: 'Optoelectronic properties of InGaAs/InGaAsP multiple-quantum-well waveguide photodetectors'. Tech. dig., 1989, LEOS Annual Meeting, Orlando, FL, 1989, Paper OE14.3

7 KOREN, U., KOCH, T. L., MILLER, B. I., and SHAHAR, A.: 'Processes for large scale photonic integrated circuits'. Tech. dig., Topical meeting on integrated and guided-wave optics, 1989, Houston, TX, pp. 68–71

EXPERIMENTAL DETERMINATION OF CARRIER-INDUCED DIFFERENTIAL LOSS IN 2-SECTION GaInAsP/InP LASER-WAVEGUIDE

Indexing terms: Semiconductor lasers, Optical waveguides, Integrated optics

Measurements of threshold crrent density and external efficiency on broad-area laser-waveguide structure have led to the determination of the optical loss and differential loss $d\alpha/dN \simeq 1{\cdot}1$–$2{\cdot}3 \times 10^{-17}\,cm^2$ at $\lambda = 1{\cdot}53\,\mu m$ in a $\lambda_g = 1{\cdot}30\,\mu m$ GaInAsP layer. This measurement will be useful for the design of tunable lasers.

Introduction: Narrow-linewidth integrated tunable lasers are key components for tunable transmitters and tunable local oscillators in coherent systems. Wavelength tuning is achieved by current injection in a passive Bragg reflector and a phase control section.[1]

The best results so far have been obtained in a 3-section DBR laser with a continuous tuning range of 3·4 nm and 17 MHz spectral linewidth.[2] The main limitation on linewidth[3] and maximum tuning range capability is due to carrier-induced absorption.

The design of optimised tunable lasers requires investigation into absorption of guided light in the passive sections. To our knowledge, only limited data have been reported for optical absorption in GaInAsP compounds.[4,5] In this letter we report a simple technique to determine the absorption and its dependence on the injected carrier density.

Experimental results: Measurements have been carried out on the 2-section broad-area laser (100 μm width) shown in the inset of Fig. 1. The structure consists of a GaInAsP ($\lambda_g = 1{\cdot}30\,\mu m$) guide layer (thickness $d_2 = 0{\cdot}14\,\mu m$, *n*-type doped, $n = 1 \times 10^{18}\,cm^{-3}$) LPE-grown on an $n = 2 \times 10^{18}\,cm^{-3}$ InP substrate, a GaInAsP ($\lambda_g = 1{\cdot}53\,\mu m$, thickness $d_1 = 0{\cdot}09\,\mu m$, undoped) layer limited to the laser section, and an InP ($p = 1 \times 10^{18}\,cm^{-3}$) cladding layer. An InP undoped stop-etch layer 0·07 μm thick is located between the active and guide layers. $L_1 = 280\,\mu m$ and L_2 are the lengths of the active and passive sections, respectively. The series resistance was $\leq 1\,\Omega$ between one electrode and the substrate and $\simeq 50\,\Omega$ between electrodes.

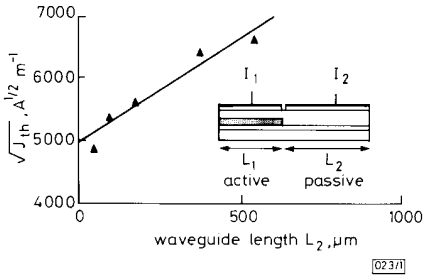

Fig. 1 *Laser-waveguide structure and square-root of threshold current density against passive waveguide length for $J_2 = 0$*

We have measured under pulsed conditions the threshold current density J_{th} against the length L_2 for current density $J_2 = 0$ in the passive section (Fig. 1), and J_{th} and external efficiency η for a given length L_2 (90, 170, 370 μm) against current density J_2 in the passive section (Fig. 2).

Analysis of experimental results: A simple analysis of these measurements leads to the determination of the modal optical loss $\alpha_{wg}(0)$ in the passive section for $J_2 = 0$ and the differential material loss $d\alpha/dN$ of the guide layer of the passive section with injected carriers *N* at $\lambda = 1{\cdot}5\,\mu m$.

Neglecting the reflections between the two sections (small effective index mismatch), it can be shown that J_{th} and η are given by

$$\sqrt{(J_{th})} = \sqrt{(J_{th0})} + \frac{1}{\Gamma_1}\frac{\sqrt{(ed_1B_1)}}{a - K_0}\left[\frac{1}{L_1}\ln\frac{1}{C} + \frac{L_2}{L_1}\alpha_{wg}(0)\right] \quad (1)$$

$$\frac{1}{\eta} = \frac{1}{\eta_0} + \left[1 + \frac{K_0}{a - K_0}\right]\left\{\frac{\ln(C^{-1}) + \alpha_{wg}(0)L_2}{\ln(R^{-1})}\right\} \quad (2)$$

where J_{th0} and η_0 represent the threshold current density and external efficiency of the solitary laser of length L_1, B_1 is the effective recombination coefficient, *a* the gain coefficient and K_0 the absorption loss coefficient (IVBA[5]) in the laser section, *R* the reflectivity of the facets, and *C* the coupling efficiency between sections. In eqns. 1 and 2 we have assumed a quadratic recombination $J \propto N^2$. The threshold current density of solitary lasers of same length $L_1 = 280\,\mu m$ was about the same as the extrapolated J_{th} of the laser-waveguide for $L_2 = 0$. The difference in J_{th} was smaller than experimental error, and we estimate a coupling efficiency $C \simeq 0{\cdot}9$ from the calculated field overlap integral. Measurements of J_{th} and η for different values of L_2 and $J_2 = 0$ lead to $\alpha_{wg}(0) \simeq 20$–$30\,cm^{-1}$, using the values of Reference 6 for the parameters of eqns. 1 and 2. A fraction of $\alpha_{wg}(0)$ is due to scattering loss α_s at the layer interfaces; typical values for LPE are $\alpha_s = 10$–$25\,cm^{-1}$;[6]